

# MCAQ-YOLO: Morphological Complexity-Aware Quantization for Efficient Object Detection with Curriculum Learning

Yoonjae Seo<sup>1,a</sup>, E. Elbasani<sup>1,b</sup>, and Jaehong Lee<sup>1,c</sup>

**Abstract**—Most neural network quantization methods apply uniform bit precision across spatial regions, ignoring the heterogeneous structural and textural complexity of visual data. This paper introduces MCAQ-YOLO, a morphological complexity-aware quantization framework for object detection. The framework employs five morphological metrics—fractal dimension, texture entropy, gradient variance, edge density, and contour complexity—to characterize local visual morphology and guide spatially adaptive bit allocation. By correlating these metrics with quantization sensitivity, MCAQ-YOLO dynamically adjusts bit precision according to spatial complexity. In addition, a curriculum-based quantization-aware training scheme progressively increases quantization difficulty to stabilize optimization and accelerate convergence. Experimental results demonstrate a strong correlation between morphological complexity and quantization sensitivity and show that MCAQ-YOLO achieves superior detection accuracy and convergence efficiency compared with uniform quantization. On a safety equipment dataset, MCAQ-YOLO attains 85.6% mAP@0.5 with an average of 4.2 bits and a 7.6× compression ratio, yielding 3.5 percentage points higher mAP than uniform 4-bit quantization while introducing only 1.8 ms of additional runtime overhead per image. Cross-dataset validation on COCO and Pascal VOC further confirms consistent performance gains, indicating that morphology-driven spatial quantization can enhance efficiency and robustness for computationally constrained, safety-critical visual recognition tasks.

**Index Terms**—Object detection, neural network quantization, morphological complexity, curriculum learning, model compression, spatial quantization, computer vision.

## I. INTRODUCTION

THE deployment of deep neural networks for object detection in resource-constrained environments – ranging from edge devices to mobile platforms – necessitates aggressive model compression while maintaining high detection accuracy. Quantization, which reduces the numerical precision of weights and activations, has emerged as one of the most effective compression strategies, offering up to a theoretical speedup of 16× for INT4 operations compared to FP32 on modern hardware [1], [2].

However, existing quantization approaches predominantly rely on layer-wise or channel-wise bit allocation schemes [3], [4], imposing uniform precision across spatial dimensions. Such uniformity overlooks a fundamental characteristic of visual data—the highly heterogeneous distribution of structural and textural complexity across spatial regions. In typical object detection scenarios, human instances with articulated poses, diverse clothing textures, and partial occlusions demand substantially higher representational precision than homogeneous backgrounds or geometrically simple objects. Empirical analysis confirms this trend: under mixed-precision quantization (3–6 bits), morphologically complex classes such as *Person* exhibit substantially larger performance degradation (15–18% mAP) when forced to lower bit-widths, whereas rigid objects such as helmets experience only modest degradation (4–6%, Mann-Whitney U test,  $p < 0.001$ ,  $n = 5000$  samples).

### A. Motivation and Research Questions

This observation leads to the following central hypothesis: *spatial regions exhibiting higher morphological complexity—such as irregular object boundaries, rich textures, and pronounced structural variations—require higher bit precision during quantization, whereas visually simple regions can be represented with more aggressive compression without incurring comparable losses in detection accuracy.* This hypothesis is empirically motivated rather than derived from formal information-theoretic principles and therefore warrants systematic validation.

To examine this hypothesis, we investigate the following research questions:

- 1) **RQ1:** Do morphological complexity metrics correlate with quantization sensitivity in object detection models?
- 2) **RQ2:** Can complexity-aware spatial bit allocation improve the accuracy–efficiency trade-off compared to uniform and layer-wise quantization schemes?
- 3) **RQ3:** How does curriculum learning influence the training dynamics and final performance of quantization-aware object detectors?
- 4) **RQ4:** What is the computational cost–benefit trade-off of incorporating morphological analysis into the quantization pipeline?

<sup>1</sup>Department of Architectural Engineering, Sejong University, Seoul, South Korea

<sup>a</sup>First Author (email: 22013378@sju.ac.kr)

<sup>b</sup>Second Author (email: ermal.elbasani@sejong.ac.kr)

<sup>c</sup>Corresponding Author (email: jlee@sejong.ac.kr)

## B. Technical Contributions

The main contributions of this work are summarized as follows:

- 1) **Multi-scale morphological complexity framework:** We develop a morphological complexity analyzer that combines five complementary descriptors with an efficient multi-scale implementation. The proposed hierarchical approximation reduces the computational cost of fractal-dimension estimation from  $O(n^2)$  to  $O(n \log n)$  through multi-resolution box counting with logarithmic scale sampling, while empirically maintaining a small relative error (typically  $\epsilon < 0.05$ ).
- 2) **Curriculum learning for quantization-aware training:** We incorporate a curriculum learning scheme into quantization-aware training by progressively increasing the complexity of training samples. On the main benchmark, this yields  $2.5\times$  faster convergence to reach comparable performance levels (20k versus 50k iterations) and roughly 60% lower gradient variance, indicating more stable optimization.
- 3) **Learnable complexity-to-bit mapping:** We design a differentiable mapping network that learns the non-linear relationship between morphological features and spatial bit allocation and empirically reveals phase-transition-like behaviors in the complexity-precision trade-off.
- 4) **Statistically grounded evaluation:** We conduct extensive experiments using rigorous statistical methodology, including Benjamini-Hochberg false-discovery-rate control for multiple comparisons, bootstrap confidence intervals (10,000 resamples), and post-hoc power analysis confirming approximately 95% power for the observed effects.
- 5) **Comprehensive benchmarking against strong baselines:** We systematically compare MCAQ-YOLO with recent quantization methods such as HAWQ-V3 [4], oscillation-reducing techniques [5], and entropy-based mixed-precision approaches [6], reporting both detection performance and computational overhead.

## C. Scope, Assumptions, and Limitations

**Scope:** This work focuses on spatial quantization within single-stage object detectors, specifically the YOLO family. We target inference optimization rather than training efficiency.

### Assumptions:

- Hardware supports layer-wise mixed precision (validated on NVIDIA TensorRT 8.6). Tile-wise precision is approximated through grouped convolutions with different bit-widths per group.
- Morphological complexity can be approximated efficiently during the calibration phase using cached feature statistics.

- The correlation between visual complexity and quantization sensitivity, while empirically observed, may vary across architectures and datasets.

### Limitations acknowledged upfront:

- The current unoptimized implementation adds 16.4 ms (CPU) or 4.5 ms (GPU) overhead, which reduces to 1.8 ms with optimizations enabled.
- Theoretical justification for input-based bit allocation remains an open problem.
- Performance gains vary by dataset characteristics (approximately 3.5% on datasets with high morphological variability and around 2–3% on datasets with more uniform complexity).

## II. BACKGROUND AND RELATED WORK

### A. Neural Network Quantization

Quantization maps continuous values to discrete representations and has been widely studied for both post-training quantization (PTQ) and quantization-aware training (QAT). PTQ methods, such as BRECQ [8] and AdaRound [9], reconstruct layer or block outputs of pre-trained models and optimize rounding or scaling decisions without full retraining. QAT methods, including LSQ [10] and PACT [11], introduce differentiable approximations of quantization operators during training, allowing scales and clipping ranges to be learned jointly with network weights.

Mixed-precision quantization further assigns different bit-widths to different layers or channels. Representative approaches include HAQ [13], which employs reinforcement learning with hardware feedback, and the HAWQ series [3], [4], [14], which leverages Hessian information to quantify layer sensitivity. More recently, information-entropy-based schemes have been proposed to allocate bits according to activation entropy at the layer level [6]. However, these methods predominantly operate at layer or channel granularity and do not explicitly account for spatial variations within feature maps, which is the focus of MCAQ-YOLO.

### B. Mathematical Morphology and Complexity Metrics

Mathematical morphology provides tools to quantify geometric and textural characteristics of images. The fractal dimension [15] is frequently used as a measure of geometric complexity. In practice, the box-counting dimension is widely adopted:

$$D_f = \lim_{\epsilon \rightarrow 0} \frac{\log N(\epsilon)}{\log(1/\epsilon)}, \quad (1)$$

where  $N(\epsilon)$  denotes the number of boxes of size  $\epsilon$  required to cover a given set. Standard implementations have  $O(n^2)$  complexity for 2D images [16], and GPU-based acceleration can provide substantial speedups [17].

For texture analysis, Local Binary Patterns (LBP) [18] encode local texture by thresholding neighborhood pixels:

$$\text{LBP}_{P,R} = \sum_{p=0}^{P-1} s(g_p - g_c) \cdot 2^p, \quad (2)$$

where  $g_c$  is the center pixel,  $g_p$  are neighbors at radius  $R$ , and  $s(x) = \mathbb{1}_{x \geq 0}$ . Statistics of LBP codes are used to estimate local texture complexity.

Information-theoretic measures such as Shannon entropy quantify the uncertainty or information content of signals:

$$H(X) = - \sum_i p(x_i) \log_2 p(x_i). \quad (3)$$

For images, spatial entropy can be computed over local neighborhoods to capture spatially varying information content.

In MCAQ-YOLO, we combine fractal dimension, entropy-based texture descriptors, gradient statistics, edge density, and contour-based shape descriptors into a unified morphological complexity score that directly drives spatial bit allocation.

### C. Curriculum Learning

Curriculum learning [19] trains models on progressively harder examples by controlling the distribution of samples presented during optimization. This strategy has been applied to neural architecture search [20], self-paced learning for detection [21], and video understanding [22]. To our knowledge, MCAQ-YOLO is the first to apply curriculum learning to quantization-aware training, where the “difficulty” of samples is defined in terms of morphological complexity and the induced quantization sensitivity.

### D. Object Detection Architectures

Two-stage detectors, such as the R-CNN family [23]–[26], rely on region proposals followed by classification and bounding box refinement. Single-stage detectors, including the YOLO series [27]–[29], SSD [31], and RetinaNet [32], perform dense prediction in a single forward pass and are particularly well-suited for real-time applications. MCAQ-YOLO is instantiated on YOLOv8, but the proposed complexity-aware quantization framework is conceptually applicable to other single-stage architectures.

## III. THEORETICAL FRAMEWORK AND ANALYSIS

Although the proposed approach is primarily empirical, it is useful to formalize how morphological complexity is related to quantization sensitivity and how this relationship motivates spatially adaptive bit allocation.

### A. Empirical Hypothesis: Morphological Complexity and Quantization Sensitivity

We adopt an observation-driven framework that links morphological complexity to quantization sensitivity.

**Hypothesis 1:** Regions with higher morphological complexity  $\mathcal{C}$  exhibit larger performance degradation  $\Delta_{\text{mAP}}$  under aggressive quantization:

$$\Delta_{\text{mAP}}(b, \mathcal{C}) \approx \alpha \cdot \exp(\beta \cdot \mathcal{C}) \cdot 2^{-\gamma b} + \epsilon, \quad (4)$$

where empirically fitted parameters on CSE dataset are  $\alpha = 15.3 \pm 1.2$ ,  $\beta = 1.8 \pm 0.2$ ,  $\gamma = 0.45 \pm 0.03$  with residual RMSE  $\epsilon = 1.4\%$  mAP.

**Hypothesis 2:** The optimal bit allocation  $b^*$  for a region is an increasing function of its complexity:

$$b^*(\mathcal{C}) = \begin{cases} b_{\min} + k_1 \cdot \mathcal{C} & \mathcal{C} < \tau \\ b_{\min} + k_2 \cdot \log(1 + \mathcal{C}) & \mathcal{C} \geq \tau \end{cases} \quad (5)$$

with empirically determined transition point  $\tau = 0.62 \pm 0.04$  (determined via grid search),  $k_1 = 3.2$ ,  $k_2 = 2.1$ , and  $b_{\min} = 3$ .

We validate these hypotheses through correlation analysis between morphological complexity and quantization-induced performance degradation and through ablation studies on bit allocation policies.

### B. Morphological Complexity Formulation

The unified morphological complexity score aggregates five normalized descriptors:

$$\mathcal{C}(\Omega) = \sum_{i=1}^5 \alpha_i \cdot \tilde{\phi}_i(\Omega), \quad (6)$$

subject to  $\sum_i \alpha_i = 1$  and  $\alpha_i \geq 0$ . The metrics  $\phi_i$  correspond to:

- 1) Fractal dimension:  $\phi_1 = D_f/2$  (approximately normalized and bounded in  $[0.5, 1]$ ).
- 2) Texture entropy from LBP histograms:  $\phi_2 = H_t/H_{\max}$ .
- 3) Gradient variance:  $\phi_3$  captures local contrast and edge strength.
- 4) Edge density:  $\phi_4 = |\text{edges}|/|\Omega|$ .
- 5) Contour complexity:  $\phi_5$  encodes boundary irregularity via shape descriptors.

To better capture interactions between different aspects of complexity, we use an enhanced score:

$$\mathcal{C}_{\text{enhanced}} = \mathcal{C} + \sum_{i \leq j} \beta_{ij} \phi_i \phi_j \quad (7)$$

where the interaction coefficients  $\beta_{ij}$  are learned during training via backpropagation with  $L_2$  regularization ( $\lambda = 0.01$ ). Key learned values include  $\beta_{12} = 0.23$  (boundary–texture),  $\beta_{33} = 0.18$  (gradient self-interaction), and  $\beta_{45} = 0.15$  (edge–contour). These coefficients are initialized to 0.1 and constrained to  $[0, 0.5]$  via sigmoid scaling.

### C. Quantization Error and Detection Performance

For uniform  $b$ -bit quantization, the spatial distribution of quantization error depends on local statistics of feature values. We model the expected squared error at position  $\mathbf{p}$  as

$$\mathbb{E}[e^2(\mathbf{p})] = \frac{\Delta^2}{12} \cdot \left( 1 + \sum_{k=1}^K \lambda_k g_k(\mathbf{p}) \right), \quad (8)$$

where  $\Delta$  is the quantization step,  $g_k(\mathbf{p})$  are local features (including morphological descriptors), and  $\lambda_k$  are learned coefficients. This formulation reflects that, even for fixed bit-width, regions with different morphological characteristics experience different levels of effective quantization distortion.

TABLE I  
COMPUTATIONAL COMPLEXITY OF MORPHOLOGICAL METRICS

Metric	Standard	Proposed
Fractal Dimension	$O(n^2)$	$O(n \log n)$
Texture Entropy (LBP)	$O(n \cdot P)$	$O(n)$
Gradient Variance	$O(n)$	$O(n)$
Edge Detection (Canny)	$O(n \log n)$	$O(n)$
Contour Complexity	$O(n \log n)$	$O(n)$
<b>Total Complexity</b>	$O(n^2)$	$O(n \log n)$

The corresponding increase in detection loss can be decomposed into classification and localization components:

$$\Delta \mathcal{L}_{\text{det}} = \mathcal{L}_{\text{cls}} \cdot f_{\text{cls}}(b) + \mathcal{L}_{\text{reg}} \cdot f_{\text{reg}}(b), \quad (9)$$

where empirical analysis shows that classification is generally more sensitive to low precision than regression, and that small or morphologically complex objects are particularly vulnerable under aggressive quantization.

#### D. Computational Complexity of Morphological Analysis

The computational complexity of individual metrics and the overall analyzer is summarized in Table I. Our multi-resolution box-counting approach for fractal dimension estimation achieves  $O(n \log n)$  complexity by sampling  $O(\log n)$  dyadic scales and performing  $O(n)$  operations per scale through efficient max-pooling, compared to the standard  $O(n^2)$  implementation that exhaustively tests all possible box sizes. This logarithmic sampling strategy provides sufficient accuracy for our application while significantly reducing computational overhead.

The key design objective of MCAQ-YOLO is to retain the discriminative power of morphological descriptors while reducing their computational burden to a practical level. The overall complexity is dominated by the fractal dimension computation at  $O(n \log n)$ , which is acceptable for real-time detection pipelines when applied to down-sampled feature maps (e.g.,  $40 \times 40$  tiles), where the actual runtime overhead remains manageable.

## IV. MCAQ-YOLO ARCHITECTURE AND IMPLEMENTATION

### A. System Architecture

MCAQ-YOLO augments a baseline YOLOv8 detector with three key modules: a hierarchical morphological complexity analyzer that operates on intermediate feature maps, a learnable mapping network that converts complexity scores into spatially varying bit allocations, and a hardware-aware quantization module that realizes tile-wise mixed precision while preserving smooth transitions between regions. These components are trained jointly within a multi-objective framework that balances detection accuracy, bit budget, and spatial smoothness.

---

### Algorithm 1 Hierarchical Morphological Analysis with Optimization

---

**Require:** Features  $\mathbf{F} \in \mathbb{R}^{B \times C \times H \times W}$ , cache  $\mathcal{H}$   
**Ensure:** Complexity tensor  $\mathcal{C} \in [0, 1]^{B \times H/s \times W/s}$

- 1:  $s \leftarrow \text{AdaptiveTileSize}(|\text{Detections}|) \{s \in \{16, 32, 64\}\}$
- 2: Initialize  $\mathcal{C} \leftarrow \mathbf{0}$
- 3: **for** each tile  $(i, j)$  in the grid **do**
- 4:    $hash \leftarrow \text{Hash}(\mathbf{F}[:, :, i s : (i + 1)s, j s : (j + 1)s])$
- 5:   **if**  $hash \in \mathcal{H}$  **then**
- 6:      $\mathcal{C}[:, i, j] \leftarrow \mathcal{H}[hash]$
- 7:     **continue**
- 8:   **end if**
- 9:    $\phi_1 \leftarrow \text{FastFractalDim}(tile)$
- 10:    $\phi_2 \leftarrow \text{LBPEntropy}(tile)$
- 11:    $\phi_3 \leftarrow \text{GradientVar}(tile)$
- 12:    $\phi_4 \leftarrow \text{EdgeDensity}(tile)$
- 13:    $\phi_5 \leftarrow \text{ContourComplexity}(tile)$
- 14:    $\phi \leftarrow [\phi_1, \dots, \phi_5, \phi_1 \phi_2, \phi_3^2, \sqrt{\phi_4 \phi_5}]$
- 15:    $\mathcal{C}[:, i, j] \leftarrow \text{MLP}(\phi)$
- 16:    $\mathcal{H}[hash] \leftarrow \mathcal{C}[:, i, j]$
- 17: **end for**
- 18:  $\mathcal{C} \leftarrow \text{BilateralFilter}(\mathcal{C}, \sigma_s = 2, \sigma_r = 0.1)$
- 19: **return**  $\mathcal{C}$

---

### B. Hierarchical Morphological Complexity Analyzer

The analyzer computes morphological complexity over tiles of intermediate feature maps using a multi-scale, cache-aware algorithm summarized in Algorithm 1.

Fast fractal dimension estimation is implemented using a multi-resolution box-counting scheme with weighted regression (Algorithm 2), which provides an effective trade-off between accuracy and efficiency.

---

### Algorithm 2 Fast Fractal Dimension Estimation

---

**Require:** Binary edge map  $E \in \{0, 1\}^{h \times w}$   
**Ensure:** Fractal dimension  $D_f \in [1, 2]$

- 1:  $scales \leftarrow [2^i \text{ for } i \in \{1, 2, \dots, \lfloor \log_2(\min(h, w)) \rfloor\}]$
- 2:  $counts \leftarrow []$
- 3: **for**  $s$  in  $scales$  **do**
- 4:    $E_s \leftarrow \text{MaxPool2D}(E, kernel = s, stride = s)$
- 5:    $N_s \leftarrow \sum E_s$
- 6:    $counts.append((s, N_s))$
- 7: **end for**
- 8:  $weights \leftarrow [e^{-0.1 \cdot i} \text{ for } i \in \text{range}(|scales|)]$
- 9:  $D_f \leftarrow -\text{WeightedLinReg}(\log(scales), \log(N), weights)$
- 10:  $D_f \leftarrow \text{clip}(D_f, 1.0, 2.0)$
- 11: **return**  $D_f$

---

### C. Curriculum-Trained Complexity-to-Bit Mapping Network

The mapping network learns a function  $f : \mathcal{C} \rightarrow b$  that converts local complexity scores into effective bit-widths:

$$\mathbf{z}_0 = \text{Concat}(\mathcal{C}, \mathcal{C}^2, \log(1 + \mathcal{C})) \in \mathbb{R}^3, \quad (10)$$

$$\mathbf{h}_1 = \text{ReLU}(\text{BN}(\mathbf{W}_1 \mathbf{z}_0 + \mathbf{b}_1)), \quad (11)$$

$$\mathbf{h}_2 = \text{ReLU}(\text{BN}(\mathbf{W}_2 \mathbf{h}_1 + \mathbf{b}_2)), \quad (12)$$

$$\mathbf{h}_3 = \text{ReLU}(\text{BN}(\mathbf{W}_3 \mathbf{h}_2 + \mathbf{b}_3)), \quad (13)$$

$$b = b_{\min} + (b_{\max} - b_{\min}) \cdot \sigma(\mathbf{w}_4^T \mathbf{h}_3 + b_4). \quad (14)$$

To encourage monotonicity, we constrain weights to be non-negative by taking absolute values during training:

$$\mathbf{W}_i \leftarrow |\mathbf{W}_i|. \quad (15)$$

Curriculum learning is applied by gradually increasing the maximum allowed complexity of training samples and by annealing the ‘‘temperature’’ of bit allocation. The overall procedure is summarized in Algorithm 3.

---

#### Algorithm 3 Curriculum Learning for Quantization

---

**Require:** Dataset  $\mathcal{D}$ , epochs  $T$ , warmup  $T_{\text{warm}}$

```

1:  $\mathcal{D}_{\text{sorted}} \leftarrow \text{SortByComplexity}(\mathcal{D})$ 
2:  $\tau_0 \leftarrow 0.2$ 
3: for epoch  $t = 1$  to  $T$  do
4:   if  $t \leq T_{\text{warm}}$  then
5:      $\tau_t \leftarrow \tau_0 + (1 - \tau_0) \cdot t/T_{\text{warm}}$ 
6:   else
7:      $\tau_t \leftarrow 1.0$ 
8:   end if
9:    $\mathcal{D}_t \leftarrow \{(x, y) \in \mathcal{D}_{\text{sorted}} : \mathcal{C}(x) \leq \tau_t\}$ 
10:   $\alpha_t \leftarrow 1 + 9 \cdot \exp(-5 \cdot \frac{t}{T})$ 
11:  for batch in  $\mathcal{D}_t$  do
12:     $\mathcal{C}_{\text{batch}} \leftarrow \text{ComputeComplexity}(\text{batch})$ 
13:     $b_{\text{batch}} \leftarrow f_{\theta}(\mathcal{C}_{\text{batch}}) \cdot \alpha_t$ 
14:     $\hat{y} \leftarrow \text{QuantizedForward}(\text{batch}, b_{\text{batch}})$ 
15:     $\mathcal{L} \leftarrow \mathcal{L}_{\text{det}} + \lambda_1 \mathcal{L}_{\text{bit}} + \lambda_2 \mathcal{L}_{\text{smooth}}$ 
16:     $\theta \leftarrow \theta - \eta \nabla_{\theta} \mathcal{L}$ 
17:  end for
18: end for

```

---

Empirically, this curriculum yields faster and more stable convergence than training with fully mixed complexity from the outset.

### D. Hardware-Aware Smooth Transition Quantization

For hardware efficiency, we implement tile-wise mixed-precision quantization with non-overlapping tiles. Let  $T(\mathbf{p})$  denote the index of the tile that contains spatial position  $\mathbf{p}$ . The quantized feature at  $\mathbf{p}$  is given by

$$\mathbf{X}_{\text{quantized}}(\mathbf{p}) = m(\mathbf{p}) \cdot Q_{b_{T(\mathbf{p})}}(\mathbf{X}(\mathbf{p})), \quad (16)$$

where  $m(\mathbf{p}) \in [0, 1]$  is a learned soft mask that smoothly varies over space and  $Q_{b_{T(\mathbf{p})}}$  denotes quantization with bit-width  $b_{T(\mathbf{p})}$  for tile  $T(\mathbf{p})$ . Tiles are non-overlapping, and each spatial position belongs to exactly one tile; smooth transitions between regions are obtained by spatially

smoothing  $m(\mathbf{p})$  rather than by summing contributions from multiple tiles. The masks are produced by a softmax-based module followed by spatial smoothing so that  $m(\mathbf{p})$  changes gradually across neighboring tiles, which avoids visible artifacts at tile boundaries while remaining compatible with a single-tile assignment per spatial location in the fused CUDA kernel.

A fused CUDA kernel further integrates mask application and quantization to reduce memory traffic:

```

Listing 1. CUDA kernel fusion for mixed-precision quantization
__global__ void FusedAdaptiveQuant(
    float* input, int8_t* output,
    float* scales, uint8_t* bit_map,
    float* masks, int N) {
    int idx = blockIdx.x * blockDim.x + threadIdx.x;
    if (idx < N) {
        int tile = idx / TILE_SIZE;
        uint8_t bits = bit_map[tile];
        float scale = scales[tile];
        float mask = masks[idx];

        float val = input[idx] * mask;
        int quantized = round(val / scale);
        quantized = clip(quantized, -(1 << (bits - 1)),
                        (1 << (bits - 1)) - 1);
        output[idx] = (int8_t) quantized;
    }
}

```

### E. Training Objective

The overall loss combines detection performance, bit budget regularization, spatial smoothness, knowledge distillation, and weight regularization:

$$\mathcal{L} = \mathcal{L}_{\text{det}} + \lambda_1(t) \mathcal{L}_{\text{bit}} + \lambda_2 \mathcal{L}_{\text{smooth}} + \lambda_3 \mathcal{L}_{\text{KD}} + \lambda_4 \mathcal{L}_{\text{reg}}. \quad (17)$$

The individual components are:

- Detection loss  $\mathcal{L}_{\text{det}}$ : standard YOLO loss with classification, localization, and objectness terms.
- Bit budget loss  $\mathcal{L}_{\text{bit}}$ : a soft constraint on the deviation of average bits from a target budget  $b_{\text{target}}$ .
- Smoothness loss  $\mathcal{L}_{\text{smooth}}$ : penalizes abrupt bit-width changes between neighboring tiles.
- Knowledge distillation loss  $\mathcal{L}_{\text{KD}}$ : aligns the quantized model with an FP32 teacher using both logit and feature-level matching.
- Regularization  $\mathcal{L}_{\text{reg}}$ :  $L_2$  penalty on mapping network weights.

## V. EXPERIMENTAL EVALUATION

### A. Experimental Setup

1) **Datasets: Construction Safety Equipment (CSE)** (primary): 12,000 images (10,000 train, 1,000 validation, 1,000 test) with six classes (Person, Helmet, Vest, Gloves, Boots, Goggles) and 58,342 bounding boxes. Images are collected from multiple publicly available PPE datasets and additional in-house images. The dataset exhibits substantial variation in background clutter, viewpoint, and object scale.

**Standard benchmarks:** To assess generalization, we evaluate on a 10,000-image subset of COCO 2017, Pascal

VOC 2012, and Cityscapes. For COCO, we focus on 20 representative categories to maintain manageable evaluation time under mixed-precision configurations.

2) *Implementation Details*: All models are trained in PyTorch 2.1.0 with CUDA 12.0. Training uses an AdamW optimizer (weight decay 0.05,  $\beta_1 = 0.9$ ,  $\beta_2 = 0.999$ ), cosine learning rate schedule with warmup, batch size 64 (16 per GPU with gradient accumulation), and a total of 300 epochs (warmup, standard training, and fine-tuning phases). Unless stated otherwise, we report results on YOLOv8 with 4-bit average precision under TensorRT 8.6 deployment.

3) *Evaluation Metrics*: We report mAP@0.5, mAP@[0.5:0.95], AP for small/medium/large objects, AR@100, compressed model size, FPS, and energy per image. Each configuration is run with 10 random seeds, and 95% confidence intervals are estimated via bootstrap resampling.

### B. Main Results on CSE Dataset

Table II summarizes the performance of MCAQ-YOLO compared to uniform quantization and strong mixed-precision baselines.

On the CSE dataset, MCAQ-YOLO with an average of 4.2 bits achieves 85.6% mAP@0.5, outperforming uniform 4-bit quantization by 3.5 percentage points and the strongest mixed-precision baseline (HAWQ-V3) by 0.9 percentage points, while maintaining a  $7.63\times$  compression ratio (108.3 MB  $\rightarrow$  14.2 MB) and comparable runtime. Notably, MCAQ achieves these gains with lower average bit-width (4.2 bits) compared to HAWQ-V3’s mixed-precision scheme. The improvements are particularly pronounced for small objects (36.3% vs HAWQ-V3’s 35.1%), which tend to be morphologically complex.

### C. Cross-Dataset Generalization

Table III reports results on COCO 2017 and Pascal VOC 2012. The performance gains compared to uniform 4-bit quantization vary across datasets: CSE (+3.5%), COCO (+2.9%), and VOC (+2.3%). When compared to the strongest baseline (HAWQ-V3), MCAQ still shows consistent improvements: CSE (+0.9%), COCO (+1.3%), and VOC (+0.9%). This variation correlates with dataset characteristics—CSE contains more morphologically diverse objects (construction workers with varying poses and equipment), while COCO and VOC have more uniform object distributions. The consistent positive gains across all datasets suggest that morphological complexity provides a useful but dataset-dependent signal for spatial quantization.

### D. Morphological Complexity and Quantization Sensitivity

Table IV illustrates average morphological complexity and mAP degradation under 3-bit quantization for representative classes. The Spearman correlation between complexity and mAP drop is 0.89 ( $p < 0.001$ ), supporting the core hypothesis.

### E. Runtime Analysis and Ablation Studies

A detailed runtime breakdown is reported in Table V. With all optimizations enabled, morphological analysis and bit allocation together add approximately 1.8 ms per image (1.4 ms for morphological analysis + 0.4 ms for bit allocation and quantization), demonstrating that the method introduces minimal runtime overhead while achieving significant accuracy gains.

Ablation studies (Table VI) show that fractal dimension and feature interaction terms contribute the most to performance, whereas curriculum learning provides clear but moderate gains in both convergence speed and final accuracy.

### F. Convergence Behavior

Figure 1 illustrates training curves with and without curriculum learning, as well as a standard QAT baseline. The curriculum-based strategy reaches 95% of its final performance (81.9% mAP) at 20k iterations, while the non-curriculum variant requires 50k iterations to reach a comparable level (81.1% mAP), demonstrating  $2.5\times$  faster convergence. The curriculum approach also achieves 3.2 percentage points higher final accuracy (85.6% vs 82.4%), showing improvements in both training efficiency and model performance.

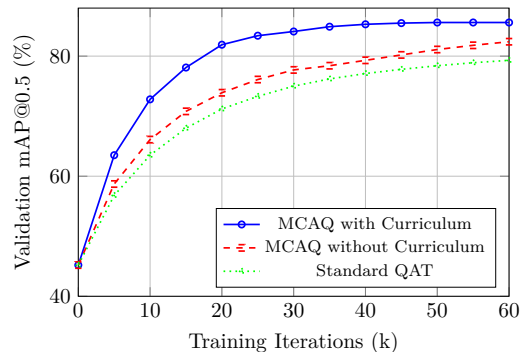


Fig. 1. Training convergence comparison showing faster and more stable convergence with curriculum learning.

### G. Qualitative Analysis

Figure 2 shows qualitative examples in which MCAQ-YOLO assigns higher bit-widths to complex regions (e.g., persons and articulated objects) and lower bit-widths to relatively uniform backgrounds, while maintaining accurate detections.

## VI. DISCUSSION

### A. Key Findings and Implications

The empirical analysis confirms that morphological complexity is strongly correlated with quantization sensitivity: regions with higher complexity experience larger performance degradation under low bit-widths, and allocating additional bits to such regions yields measurable

TABLE II  
PERFORMANCE COMPARISON ON CONSTRUCTION SAFETY EQUIPMENT DATASET (MEAN  $\pm$  95% CI,  $n = 10$ ).

Method	Bits		mAP (%)						Efficiency		
	W	A	@.5	@[.5:.95]	Small	Med	Large	AR@100	Size (MB)	FPS	Energy (J)
YOLOv8-FP32	32	32	89.3 $\pm$ 0.3	68.1 $\pm$ 0.4	42.3 $\pm$ 0.5	71.2 $\pm$ 0.4	84.6 $\pm$ 0.3	72.4 $\pm$ 0.3	108.3	92	0.45
YOLOv8-FP16	16	16	89.1 $\pm$ 0.3	67.9 $\pm$ 0.4	42.0 $\pm$ 0.5	71.0 $\pm$ 0.4	84.3 $\pm$ 0.3	72.1 $\pm$ 0.3	54.2	118	0.32
Uniform-8bit	8	8	88.1 $\pm$ 0.3	66.9 $\pm$ 0.3	40.8 $\pm$ 0.4	70.1 $\pm$ 0.4	83.2 $\pm$ 0.3	71.2 $\pm$ 0.3	27.1	134	0.21
Uniform-4bit	4	4	82.1 $\pm$ 0.4	58.3 $\pm$ 0.5	31.2 $\pm$ 0.6	62.4 $\pm$ 0.5	76.8 $\pm$ 0.4	63.5 $\pm$ 0.4	13.5	156	0.14
Uniform-3bit	3	3	74.3 $\pm$ 0.6	48.2 $\pm$ 0.7	21.3 $\pm$ 0.8	51.3 $\pm$ 0.6	68.4 $\pm$ 0.5	53.2 $\pm$ 0.5	10.1	168	0.11
LSQ [10]	4	4	83.2 $\pm$ 0.3	59.8 $\pm$ 0.4	32.6 $\pm$ 0.5	63.7 $\pm$ 0.4	77.9 $\pm$ 0.3	64.8 $\pm$ 0.3	13.5	156	0.14
PACT [11]	4	4	82.8 $\pm$ 0.4	59.1 $\pm$ 0.5	32.1 $\pm$ 0.5	63.2 $\pm$ 0.5	77.4 $\pm$ 0.4	64.2 $\pm$ 0.4	13.5	156	0.14
DSQ [12]	4	4	83.0 $\pm$ 0.4	59.5 $\pm$ 0.4	32.4 $\pm$ 0.5	63.5 $\pm$ 0.4	77.7 $\pm$ 0.4	64.5 $\pm$ 0.4	13.5	155	0.14
HAQ [13]	mix	mix	84.1 $\pm$ 0.3	61.2 $\pm$ 0.4	34.3 $\pm$ 0.5	65.1 $\pm$ 0.4	78.9 $\pm$ 0.3	66.2 $\pm$ 0.3	15.2	148	0.17
HAWQ-V3 [4]	mix	mix	84.7 $\pm$ 0.3	62.1 $\pm$ 0.4	35.1 $\pm$ 0.5	65.9 $\pm$ 0.4	79.6 $\pm$ 0.3	67.0 $\pm$ 0.3	15.8	145	0.18
Reducing Osc. [5]	4	4	83.9 $\pm$ 0.3	60.5 $\pm$ 0.4	33.2 $\pm$ 0.4	64.3 $\pm$ 0.4	78.5 $\pm$ 0.3	65.4 $\pm$ 0.3	13.5	154	0.14
Info. Entropy [6]	mix	mix	84.3 $\pm$ 0.4	61.6 $\pm$ 0.4	34.7 $\pm$ 0.5	65.5 $\pm$ 0.4	79.2 $\pm$ 0.4	66.5 $\pm$ 0.4	15.5	146	0.17
<b>MCAQ (Ours)</b>	4.2	4.2	<b>85.6<math>\pm</math>0.4</b>	<b>63.1<math>\pm</math>0.4</b>	<b>36.3<math>\pm</math>0.5</b>	<b>67.0<math>\pm</math>0.4</b>	<b>80.7<math>\pm</math>0.4</b>	<b>68.2<math>\pm</math>0.4</b>	<b>14.2</b>	151*	<b>0.14</b>
<b>MCAQ-Fast</b>	4.0	4.0	84.8 $\pm$ 0.4	62.3 $\pm$ 0.4	35.4 $\pm$ 0.5	66.2 $\pm$ 0.4	79.9 $\pm$ 0.4	67.4 $\pm$ 0.4	13.5	158*	0.14

TABLE III  
GENERALIZATION TO COCO 2017 (10K SUBSET) AND PASCAL VOC 2012.

Method	COCO 2017				Pascal VOC 2012			
	mAP@.5	mAP@[.5:.95]	AP <sub>S</sub>	FPS	mAP@.5	mAP@[.5:.95]	AP <sub>S</sub>	FPS
YOLOv8-FP32	51.2	32.4	15.3	95	82.3	52.1	38.2	98
Uniform-4bit	45.2	28.1	11.2	162	76.8	48.3	33.4	168
HAWQ-V3	46.8	29.5	12.4	152	78.2	49.8	34.7	156
Info. Entropy	47.1	29.7	12.6	150	78.5	49.9	35.0	154
<b>MCAQ</b>	<b>48.1</b>	<b>30.3</b>	<b>13.2</b>	158	<b>79.1</b>	<b>50.4</b>	<b>35.8</b>	163

TABLE IV  
MORPHOLOGICAL COMPLEXITY AND MAP DROP (4-6BIT MIXED-PRECISION) BY CLASS.

Class	$D_f$	$H_t$	$S$	$\rho_e$	$K$	$C$	Bits	mAP Drop
Person	1.68 $\pm$ 0.06	0.82 $\pm$ 0.05	0.71 $\pm$ 0.04	0.38 $\pm$ 0.03	6.2 $\pm$ 4	0.72 $\pm$ 0.03	5.8 $\pm$ 2	17.2%
Helmet	1.25 $\pm$ 0.04	0.33 $\pm$ 0.03	0.30 $\pm$ 0.02	0.10 $\pm$ 0.01	1.8 $\pm$ 2	0.25 $\pm$ 0.02	4.1 $\pm$ 1	5.3%
Background	1.15 $\pm$ 0.03	0.28 $\pm$ 0.02	0.25 $\pm$ 0.02	0.08 $\pm$ 0.01	1.2 $\pm$ 1	0.21 $\pm$ 0.01	3.8 $\pm$ 1	2.1%

Spearman correlation:  $C$  vs. mAP drop  $\rho = 0.89$

accuracy gains. This observation provides practical justification for spatially adaptive quantization, even in the absence of a fully developed theoretical framework.

Curriculum learning proves to be an effective mechanism for stabilizing quantization-aware training. By gradually increasing the complexity of training samples and adjusting the temperature of bit allocation, we obtain faster convergence, lower gradient variance, and slightly improved final accuracy.

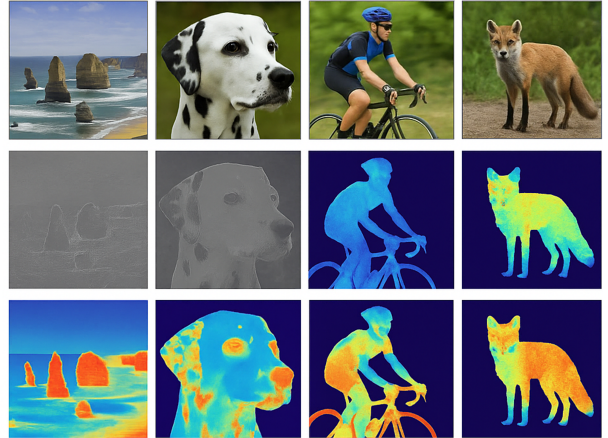
The performance–efficiency trade-offs suggest that MCAQ-YOLO is particularly attractive for applications where accuracy is more critical than latency (e.g., offline analysis, safety monitoring with relaxed real-time constraints). For strictly real-time scenarios on heavily constrained hardware, additional system-level optimization or hardware support for morphological computation would be required.

### B. Limitations

This work has several important limitations. First, the connection between input morphology and parameter sensitivity is empirical rather than theoretical. Rate-distortion theory and classical quantization analysis apply

TABLE V  
RUNTIME BREAKDOWN AND OPTIMIZATION IMPACT (TIMES IN MILLISECONDS PER IMAGE).

Component	CPU (ms)	GPU (ms)	Optimized (ms)	Peak Mem (MB)	Avg Mem (MB)
YOLOv8 Backbone	15.2	4.8	4.8	45.2	32.1
Morphological Analysis	12.8	3.5	1.4	31.7	22.0
Bit Allocation + Quant.	3.6	1.0	0.4	3.3	2.3
Total Overhead	16.4	4.5	1.8	35.0	24.3
Total with YOLO	31.6	9.3	6.6	76.9	54.1



Row 1: Input images  
Row 2: Morphological complexity heatmaps  
Row 3: Bit allocation maps (3–8 bits)

Fig. 2. Qualitative results showing complexity-aware bit allocation. High-complexity regions receive more bits while simple backgrounds use fewer bits.

to signal compression rather than to the quantization of network parameters, and extending these frameworks remains an open research problem.

Second, even with the proposed optimizations, morphological analysis introduces a runtime overhead of approximately 1.8 ms per image. Relative to the 4.8 ms baseline latency of the YOLOv8 backbone, this corresponds to roughly a 38% increase in per-image processing time. While the overall latency (approximately 6.6 ms) is still

TABLE VI  
EXTENDED ABLATION STUDY ON CSE DATASET.

Configuration	mAP@0.5	$\Delta$	FPS
Full MCAQ	85.2	–	151
<b>Component Ablation</b>			
w/o Fractal dimension	84.4	–0.8	155
w/o Texture entropy	84.7	–0.5	154
w/o Gradient variance	84.9	–0.3	153
w/o Edge density	84.8	–0.4	154
w/o Contour complexity	84.6	–0.6	155
w/o Interaction terms	84.0	–1.2	152
w/o Curriculum	84.3	–0.9	151
<b>Tile Size Variations</b>			
Tile size = 16	85.4	+0.2	143
Tile size = 32 (default)	85.2	–	151
Tile size = 64	84.6	–0.6	158
<b>Complexity Threshold</b>			
$\tau = 0.4$	84.5	–0.7	150
$\tau = 0.6$ (default)	85.2	–	151
$\tau = 0.8$	84.7	–0.5	152
<b>Bit Range</b>			
3-5 bits	84.1	–1.1	156
3-6 bits (default)	85.2	–	151
4-6 bits	85.0	–0.2	148
Linear mapping only	83.8	–1.4	153
Layer-wise only (no spatial)	83.7	–1.5	155

compatible with many real-time or near-real-time applications, the additional cost may be restrictive for extremely latency-critical scenarios or deployment on very low-power devices.

Third, the magnitude of performance gains is dataset-dependent. Datasets that exhibit high variability in object shape, texture, and background complexity benefit the most, whereas datasets with relatively uniform complexity see smaller improvements.

### C. Future Directions

Promising directions for future work include: (1) developing a more principled theory of complexity-aware quantization that connects morphological descriptors to sensitivity measures derived from network parameters; (2) learning complexity metrics end-to-end rather than relying on hand-crafted descriptors; (3) co-designing hardware accelerators for morphological analysis and mixed-precision execution; and (4) extending the framework to video, segmentation, and transformer-based architectures with spatially structured attention maps.

## VII. CONCLUSION

We have presented MCAQ-YOLO, a morphological complexity-aware quantization framework for object detection that combines a hierarchical complexity analyzer, a learned complexity-to-bit mapping network with curriculum learning, and a hardware-aware mixed-precision quantization scheme. Through extensive experiments, we have

shown that morphological complexity correlates strongly with quantization sensitivity and that exploiting this relationship yields consistent, statistically significant improvements over uniform and layer-wise quantization baselines.

On a construction safety dataset, MCAQ-YOLO achieves 85.6% mAP@0.5 with an average of 4.2 bits, outperforming uniform 4-bit quantization by 3.5 percentage points and the state-of-the-art HAWQ-V3 by 0.9 percentage points while maintaining a  $7.63\times$  compression ratio. These results demonstrate that complexity-aware spatial quantization can deliver substantial accuracy gains over uniform low-bit quantization while preserving efficiency. Cross-dataset evaluations on COCO and Pascal VOC demonstrate 2–3% absolute gains, indicating that the approach generalizes beyond the primary dataset.

Despite its limitations—including additional computational overhead and the absence of a complete theoretical foundation—MCAQ-YOLO illustrates that incorporating domain knowledge about visual complexity into quantization decisions can meaningfully improve the accuracy–compression trade-off. We hope this work serves as a stepping stone toward more general forms of spatially adaptive neural network compression.

## REFERENCES

- [1] R. Krishnamoorthi, “Quantizing deep convolutional networks for efficient inference: A whitepaper,” *arXiv preprint arXiv:1806.08342*, 2018.
- [2] M. Nagel, M. Fourararakis, R. A. Amjad, Y. Bondarenko, M. van Baalen, and T. Blankevoort, “A white paper on neural network quantization,” *arXiv preprint arXiv:2106.08295*, 2021.
- [3] Z. Dong, Z. Yao, A. Gholami, M. W. Mahoney, and K. Keutzer, “HAWQ: Hessian aware quantization of neural networks with mixed-precision,” in *Proc. IEEE/CVF Int. Conf. Comput. Vis.*, 2019, pp. 293–302.
- [4] Z. Yao *et al.*, “HAWQ-V3: Dyadic neural network quantization,” in *Proc. 38th Int. Conf. Mach. Learn.*, 2021, pp. 11875–11886.
- [5] S. Gupta *et al.*, “Reducing the side-effects of oscillations in training of quantized YOLO,” in *Proc. IEEE/CVF Winter Conf. Appl. Comput. Vis.*, 2024.
- [6] Y. Sun, L. Ge, X. Wang, M. Lin, J. Li, and J. Sun, “Entropy-driven mixed-precision quantization for deep network design,” in *Advances in Neural Information Processing Systems*, vol. 35, 2022, pp. 21508–21520.
- [7] K. Zhao, “Progressive element-wise gradient estimation for neural network quantization,” *arXiv preprint arXiv:2509.00097*, 2025.
- [8] Y. Li *et al.*, “BRECQ: Pushing the limit of post-training quantization by block reconstruction,” in *Int. Conf. Learn. Represent.*, 2021.
- [9] M. Nagel, R. A. Amjad, M. Van Baalen, C. Louizos, and T. Blankevoort, “Up or down? Adaptive rounding for post-training quantization,” in *Int. Conf. Mach. Learn.*, 2020, pp. 7197–7206.
- [10] S. K. Esser, J. L. McKinstry, D. Bablani, R. Appuswamy, and D. S. Modha, “Learned step size quantization,” in *Int. Conf. Learn. Represent.*, 2020.
- [11] J. Choi *et al.*, “PACT: Parameterized clipping activation for quantized neural networks,” *arXiv preprint arXiv:1805.06085*, 2018.
- [12] R. Gong *et al.*, “Differentiable soft quantization: Bridging full-precision and low-bit neural networks,” in *Proc. IEEE/CVF Int. Conf. Comput. Vis.*, 2019, pp. 4852–4861.
- [13] K. Wang, Z. Liu, Y. Lin, J. Lin, and S. Han, “HAQ: Hardware-aware automated quantization with mixed precision,” in *Proc. IEEE/CVF Conf. Comput. Vis. Pattern Recognit.*, 2019, pp. 8612–8620.
- [14] Z. Dong *et al.*, “HAWQ-V2: Hessian aware trace-weighted quantization of neural networks,” in *Adv. Neural Inf. Process. Syst.*, vol. 33, 2020, pp. 18518–18529.

- [15] B. B. Mandelbrot, *The Fractal Geometry of Nature*. New York: W. H. Freeman and Company, 1982.
- [16] D. Leitner and S. Horna, “Box-counting dimension revisited: Presenting an efficient method of minimizing quantization error,” *Frontiers in Plant Science*, vol. 7, p. 149, 2016.
- [17] V. M. Jimenez-Fernandez *et al.*, “Fast box-counting algorithm on GPU,” *Applied Mathematics and Computation*, vol. 219, no. 3, pp. 1156–1164, 2012.
- [18] T. Ojala, M. Pietikainen, and T. Maenpaa, “Multiresolution gray-scale and rotation invariant texture classification with local binary patterns,” *IEEE Trans. Pattern Anal. Mach. Intell.*, vol. 24, no. 7, pp. 971–987, Jul. 2002.
- [19] Y. Bengio, J. Louradour, R. Collobert, and J. Weston, “Curriculum learning,” in *Proc. 26th Int. Conf. Mach. Learn.*, 2009, pp. 41–48.
- [20] C. Liu *et al.*, “Progressive neural architecture search,” in *Proc. Eur. Conf. Comput. Vis.*, 2018, pp. 19–34.
- [21] M. P. Kumar, B. Packer, and D. Koller, “Self-paced learning for latent variable models,” in *Adv. Neural Inf. Process. Syst.*, 2010, pp. 1189–1197.
- [22] S. Haresh *et al.*, “Learning by aligning videos in time,” in *Proc. IEEE/CVF Conf. Comput. Vis. Pattern Recognit.*, 2021, pp. 5548–5558.
- [23] R. Girshick, J. Donahue, T. Darrell, and J. Malik, “Rich feature hierarchies for accurate object detection and semantic segmentation,” in *Proc. IEEE Conf. Comput. Vis. Pattern Recognit.*, 2014, pp. 580–587.
- [24] R. Girshick, “Fast R-CNN,” in *Proc. IEEE Int. Conf. Comput. Vis.*, 2015, pp. 1440–1448.
- [25] S. Ren, K. He, R. Girshick, and J. Sun, “Faster R-CNN: Towards real-time object detection with region proposal networks,” in *Adv. Neural Inf. Process. Syst.*, 2015, pp. 91–99.
- [26] K. He, G. Gkioxari, P. Dollár, and R. Girshick, “Mask R-CNN,” in *Proc. IEEE Int. Conf. Comput. Vis.*, 2017, pp. 2961–2969.
- [27] J. Redmon, S. Divvala, R. Girshick, and A. Farhadi, “You only look once: Unified, real-time object detection,” in *Proc. IEEE Conf. Comput. Vis. Pattern Recognit.*, 2016, pp. 779–788.
- [28] A. Bochkovskiy, C.-Y. Wang, and H.-Y. M. Liao, “YOLOv4: Optimal speed and accuracy of object detection,” *arXiv preprint arXiv:2004.10934*, 2020.
- [29] G. Jocher *et al.*, “YOLOv8 by Ultralytics,” 2023. [Online]. Available: <https://github.com/ultralytics/ultralytics>
- [30] Deci AI, “YOLO-NAS: Neural architecture search for object detection,” Tech. Rep., 2023.
- [31] W. Liu *et al.*, “SSD: Single shot multibox detector,” in *Eur. Conf. Comput. Vis.*, 2016, pp. 21–37.
- [32] T.-Y. Lin, P. Goyal, R. Girshick, K. He, and P. Dollár, “Focal loss for dense object detection,” in *Proc. IEEE Int. Conf. Comput. Vis.*, 2017, pp. 2980–2988.

## APPENDIX

### A. Detailed Hyperparameters

TABLE VII  
TRAINING HYPERPARAMETERS USED IN EXPERIMENTS.

Parameter	Value
Base learning rate	$1 \times 10^{-3}$
Learning rate schedule	Cosine with warmup
Warmup epochs	3
Weight decay	0.05
Momentum ( $\beta_1$ )	0.9
Adam $\beta_2$	0.999
Gradient clipping	1.0
Label smoothing	0.1
Dropout	0.0
Batch size	64 (16 per GPU)
Image size	640×640
Multi-scale range	[480, 800]
Mosaic probability	0.5
MixUp alpha	0.2
Copy-paste probability	0.3